Received September 24, 2021, accepted October 18, 2021, date of publication November 2, 2021,
date of current version December 3, 2021.

Digital Object Identifier 10.1109/ACCESS.2021.3125262

Analysis and Design of an Integrated Magnetics Planar Transformer for High Power Density LLC Resonant Converter

CHUL-WAN PARK AND SANG-KYOO HAN
Power Electronics System Laboratory, POESLA, Kookmin University, Seoul 02707, South Korea

Corresponding author: Sang-Kyoo Han (djhan@kookmin.ac.kr)

This work was supported in part by the Ministry of Trade, Industry and Energy (MOTIE); in part by the Korea Institute of Energy, Technology, Evaluation, and Planning (KETEP) under Grant 2018201010650A; and in part by the Ministry of Science and ICT (MSIT), South Korea, through the Information Technology Research Center (ITRC) Support Program supervised by the Institute for Information and Communications Technology Planning and Evaluation (IITP) under Grant IITP-2021-2018-0-01396.

ABSTRACT Recent studies on compact and lightweight electronic devices have demonstrated that the LLC resonant converter (LRC) can facilitate achieving high efficiency and high power density. Moreover, employing a planar transformer can further improve the overall system power density. Although the planar transformer can assist in reducing the size of the converter, its high magnetic coupling makes the leakage inductance too small for a resonant inductor in the LRC. Therefore, an extra inductor must be employed separately, leading a considerable decrease in the power density. From this reason, significant research on integrated magnetics has been conducted to combine a transformer and external inductor into a single core. However, they require additional wires or magnetic sheets, and their structures are complex and costly. To overcome these limitations, the integrated magnetics planar transformer (IMPT) for a high power density LRC is proposed in this paper. In the proposed approach, since the primary wire is split into each side leg of the EE-type magnetic core and each operates as a transformer and a resonant inductor alternatively, an external inductor or additional wires are unnecessary. In addition, since the magnetic flux density of the IMPT is approximately equivalent to that of conventional transformer, the core size and the number of turns are almost the same. Therefore, the proposed IMPT features higher efficiency and power density without additional size and costs. To confirm the validity of the proposed IMPT, the operational principles, theoretical analysis, design considerations, and experimental results from a 350 W prototype are presented.

INDEX TERMS LLC resonant converter, planar transformer, integrated magnetics, high frequency, high-efficiency resonant converter, high power density.

NOMENCLATURE

A_o: Cross-sectional area of the side leg.
A_c: Cross-sectional area of the center leg.
N_{pi}: Number of primary turns (i = 1, 2).
N_{si}: Number of secondary turns (i = 1, 2).
g_o: Air gap of the side leg.
g_c: Air gap of the center legs.
l_o: Effective magnetic path length of the side leg.
l_c: Effective magnetic path length of the center leg.
μ_0: Permeability of the free space.
μ_r: Relative permeability of the magnetic core.
$\Re_o$: Magnetic reluctance of the outer leg.
$\Re_c$: Magnetic reluctance of the center leg.
L_{oi}: Magnetizing inductance of the side leg (i = 1, 2).
L_c: Magnetizing inductance of the center leg.
i_{pri}: Resonant current of the primary side.
i_{Loi}: Current though L_{oi}(i = 1, 2).
i_{Lc}: Current though L_c.
i_{Doi}: Current though the output diode D_{oi} (i = 1, 2).
V_{Cr}: Voltage across the resonant capacitor.
f_{sw}: Switching frequency.
f_r: Resonant frequency.
Q_e: Quality factor.

The associate editor coordinating the review of this manuscript and approving it for publication was Zhehan Yi.

n_{eq}: Equivalent turn ratio.
$H(s)$: Input-to-output voltage gain.
p: Number of copper layers.
Ψ: $\left(5p^2-1\right)/15$.
d: Thickness of the copper layer.
δ : Skin depth of the copper layer.
Δ : Ratio of the copper thickness to skin depth.
i'_{rms} : Derivative of the root mean square current.
B: Magnetic flux density.
B_m: Maximum magnetic flux density.
ρ : Resistivity ($=2.3\times10^{-6}[\Omega/cm]$).
MLT: Mean length per turn of the core.
R_{dc}: DC resistance of the wire.
R_{eff}: Effective resistance of the wire.
Φ_L : Magnetic flux of the left side leg.
Φ_R : Magnetic flux of the right side leg.
Φ_c : Magnetic flux of the center leg

I. INTRODUCTION

Today, most electronic devices and systems are not only becoming compact and lightweight but their power consumptions are also continuously increased. Therefore, high-efficiency and high-power density converters have received significant attention. For example, recent trends in the TV market require thinner and lighter TV sets, despite the demand for more power due to the increased number of pixels up to tens of millions. In order to keep up with this trend, higher-power density converters with higher efficiency are essential.

Among various power converter topologies, the LLC resonant converter (LRC) is an excellent candidate to satisfy high efficiency and high power density due to its favorable merits, such as the zero voltage switching (ZVS) of all power switches, zero current switching (ZCS) of all output rectifiers, good electromagnetic interference, and other aspects [5]–[10]. As a result, many approaches aimed at further increasing power density of the LRC have been the scope of many studies, considering these advantages.

Generally, magnetic components, such as a transformer and an inductor, are critical because they occupy a large amount of space in electronic systems. Therefore, many researches have tried to reduce the size of magnetic components, which are essential in achieving a high power density converter. Among them, increasing the switching frequency can be a good approach [1]. However, the switching losses of power semiconductors are increased in proportion to switching frequency. Although power switches with excellent performance (i.e., small parasitic capacitors, high on and off speed, small turn on resistance) have been steadily released, a limitation is still existed in reducing the size of a magnetic device by increasing only the switching frequency [2]–[4].

Meanwhile, to further reduce the size of converter, employing a planar transformer can be a good approach. In a planar transformer, the wires and bobbins can be replaced by a printed circuit board (PCB); thus, the size and thickness of a converter can be considerably reduced. However, the number of PCB layers must be increased in proportion to the number of turns. Therefore, for a large number of turns, the volume and cost may be significantly increased.

To reduce the number of PCB layers, conventional studies have proposed an integrated dual transformer (IDT) [10]. Namely, the primary wire is split in half, and each wire is placed on each side leg of the EE- or UU-type magnetic core. Thus, the separated primary turns reduce the thickness as well as the number of PCB layers [11]. However, since the high magnetic coupling of a planar transformer makes leakage inductance too small to be used as a resonant inductor in the LRC, an extra inductor must be employed and it considerably decreases the power density.

To overcome this problem, several types of integrated magnetics transformers have been proposed to integrate an external inductor into a transformer [12]–[17]. In [12], the resonant inductor is integrated with the transformer in a single magnetic core using the decoupling integration method. However, this method requires additional windings for the resonant inductor except for the main transformer, which may significantly increase the size and volume of the integrated magnetics. Moreover, since the copper wire must be wound around all legs of the magnetic core, the large number of turns can be required to achieve sufficient resonant inductance. Therefore, implementing this method with the planar transformer can significantly increase the number of PCB layers, the size of the PCB, and the magnetic core. In [13], primary wires are constructed at a spatial distance from secondary wires to obtain sufficient leakage inductance required to function as a resonant inductor. However, the spatial distance between the primary and secondary wires increases the height of the transformer. Moreover, its complex structure may not be suitable for a planar transformer. In [14], a resonant inductor and transformer are physically integrated into a single magnetic core (i.e., each one is placed on each side leg of the EE-type magnetic core, respectively). Although this approach has the advantage of a single magnetic core, it has the disadvantages of a magnetic flux imbalance in each leg and the large number of PCB layers. Namely, the primary and secondary wires of the transformer must be wound on only one of the three legs. As a result, the many PCB layers are required to implement the planar transformer. Moreover, since the flux density (B) of the resonant inductor generated by the resonant current is high, the cross-sectional area and core loss may be significantly increased. In [15], resonant inductor and transformer wires are placed together on the center leg and magnetically divided by the I-core inserted between the upper and lower E-cores of the EE-type magnetic core. Since the magnetic fluxes in the I-core generated by the transformer and resonant inductor are cancelled with each other, the flux density and subsequent core loss of the additional I-core can be reduced. However, the large number of PCB layers are still required, and additional loss and larger size from the inductor are inevitable. Especially, due to the existence of the I-core between EE-core, at least two PCBs are required to

implement a planar transformer. In [16] and [17], a magnetic sheet is inserted between the primary and secondary wires to increase the leakage inductance as a resonant inductor. Therefore, additional wire for an inductor is unnecessary, and it is easy to secure sufficient inductance for a resonant inductor. However, it is not only difficult to insert the magnetic sheet into the PCB, but there also exists a concern of high manufacturing costs.

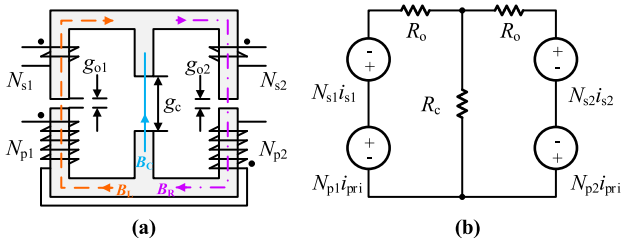

FIGURE 1. Proposed integrated magnetic planar transformer (IMPT): (a) magnetic structure, (b) reluctance model.

To overcome these limitations of prior approaches, the integrated magnetic planar transformer (IMPT) is proposed in this paper. As shown in Fig. 1(a), the split primary wire is placed on each side leg of the EE-type magnetic core, and two secondary center-tap wires are also placed on each side leg one by one. Thus, N_{p1} and N_{s1} are coupled and work as a transformer during positive half switching cycle. Further, N_{p2} functions as an inductor, because no current flows through N_{s2} due to the output rectifier. During the negative half switching cycle, the operation is inverted. Therefore, since each primary wire alternatively operates as a transformer and a resonant inductor, an external inductor or additional wires for the resonant inductor are unnecessary. Specifically, as a large resonant current flows directly through the external inductor in conventional approaches, the core loss and maximum flux density (B_m) of the inductor are high. Nevertheless, the IMPT requires no external inductor. As a result, the above-mentioned problem can be overcome. Moreover, because the flux density of the IMPT is similar to that of a conventional transformer, the core size of the transformer and its number of turns are also almost the same. Therefore, the proposed IMPT features higher efficiency and power density without additional size, cost, and power loss.

II. PROPOASED IMPT FOR THE LRC

A. EQUIVALENT INDUCTANCE MODEL OF THE PROPOSED IMPT

Fig. 1(a) illustrates the magnetic structure of the proposed IMPT, and the structure is symmetric with the air gap $g_{o1} = g_{o2} = g_o$, primary number of turns $N_{p1} = N_{p2} = N_p$, and secondary number of turns $N_{s1} = N_{s2} = N_s$. For the circuitry analysis, the physical magnetic structure can be converted into an equivalent inductance model through a reluctance model.

As depicted in Fig. 1(b), there are three magnetic paths and each path can be represented to the reluctance [18], [19]. Here, the reluctances of the side leg ($\Re_o$) and center leg ($\Re_c$) can be determined as follows:

$$\Re_o = \frac{l_o}{\mu_r \mu_0 A_o} + \frac{g_o}{\mu_0 A_o}, \quad \Re_c = \frac{l_c}{\mu_r \mu_0 A_c} + \frac{g_c}{\mu_0 A_c}. \quad (1)$$

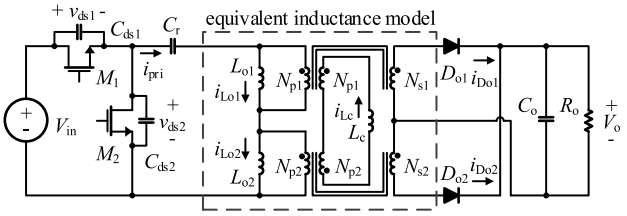

FIGURE 2. LRC configured with the equivalent inductance model of the proposed IMPT.

Generally, since μ_r is much larger than μ_0, the reluctance is mainly determined by the air gap. Then, according to the duality theory, an equivalent inductance model of the IMPT can be finally obtained and applied to the LRC as shown in Fig. 2. Each parameter of the equivalent inductance model can be determined as follows:

$$L_{o1} = L_{o2} = L_o = \frac{N_p^2}{\Re_o}, L_c = \frac{N_p^2}{\Re_c}, \quad (2)$$

where all the inductances can be adjusted by the number of primary turns and air gap.

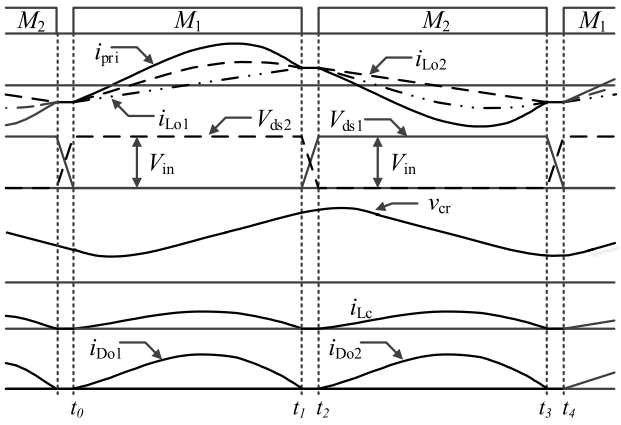

FIGURE 3. Key waveforms of the proposed IMPT LRC.

B. PRINCIPLES OF OPERATION

Fig. 2 presents the LRC configured with the equivalent inductance model of the IMPT. The key waveforms and circuit operations during one switching period are depicted in Figs. 3 and 4. The converter is operated in four modes according to the state of M_1 and M_2. Here, the M_1 is turned on and off in a complementary to M_2, and the duty ratio is fixed at about 50%. For the convenience of analysis, the following assumptions are made:

- All operations are considered in the steady state.
- The switching frequency f_{sw} is almost equal to the resonant frequency f_r.

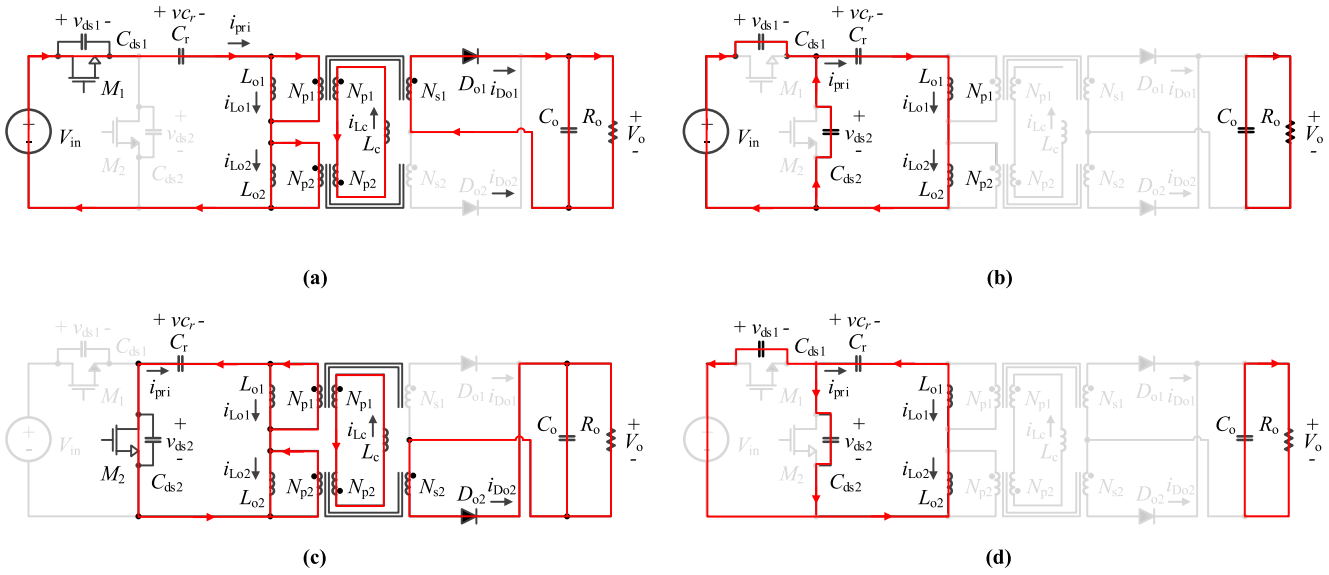

FIGURE 4. Mode operations of the proposed IMPT LRC: (a) - (d) correspond to modes 1 – 4.

- All parasitic components except those specified in Fig. 2 are neglected.
- The output capacitor C_o is large enough to be considered as a constant voltage source.
- The dead time between M_1 and M_2 is very short compared to one switching period.
- $L_{o1} = L_{o2} = L_o$, $N_{p1} = N_{p2} = N_p$, and $N_{s1} = N_{s2} = N_s$.

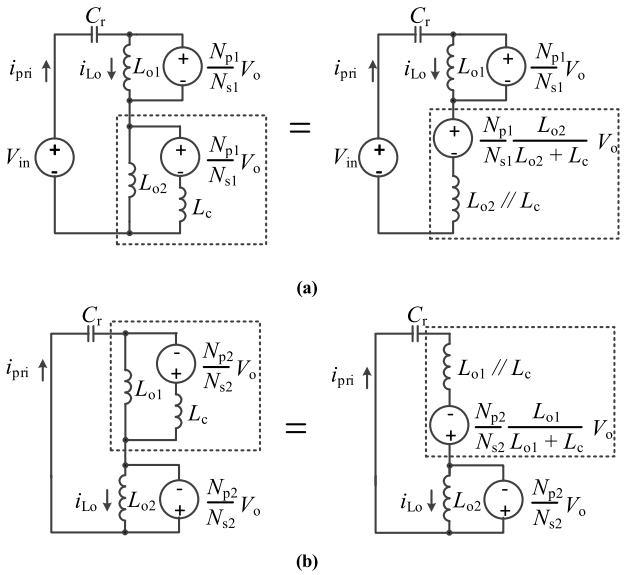

FIGURE 5. Equivalent resonant network of the IMPT: (a) mode 1 (t_0 - t_1) (b) mode 3 (t_2 - t_3).

Mode 1 (t_0 - t_1): During t_0 - t_1, M_1 is conducting and i_{pri} flows to the dot terminal of the transformer as shown in Fig. 4(a). Therefore, D_{o2} is blocked, and the input power is transferred to the output through D_{o1}. At the same time, the reflected voltage $(N_{p1}/N_{s1})V_o$ is applied to N_{p1} of the first ideal transformer; thus, series-connected L_c and $(N_{p1}/N_{s1})V_o$ are connected in parallel to L_{o2} through the second ideal transformer with the turn ratio $N_{p2} : N_{p2}$. Then, the circuit inside the dashed box on the left side of Fig. 5(a) can be simplified to Thevenin's equivalent circuit, comprising a voltage source $(N_{p1}/N_{s1})V_oL_{o2}/(L_{o2}+L_c)$ and inductor $L_{o2}||L_c$ as shown on the right side in Fig. 5(a). In the simplified circuit, N_{p1} and N_{s1} work as a transformer, whereas $L_{o2}||L_c$ acts as a resonant inductor. At this point, i_{Lo1} is increased linearly with the slope of $(N_{p1}/N_{s1})V_o/L_{o1}$, and $L_{o2}||L_c$ resonates with C_r. Here, the currents and voltages are determined as follows:

$$i_{pri}(t) = -\frac{N_p V_o T_s}{N_s 4 L_{o1}} \cos(\omega t) + \frac{\pi V_o I_o}{V_{in}} \sin(\omega t), \tag{3}$$

$$v_{C_r}(t) = V_R - \frac{N_p V_o T_s}{N_s 4 C_r \omega L_{o1}} \sin(\omega t) - \frac{V_o I_o T_s}{2 C_r V_{in}} \cos(\omega t), \tag{4}$$

$$i_{L_{o1}}(t) = -\frac{N_p V_o T_s}{N_s 4 L_{o1}} + \frac{N_p}{N_s}\frac{V_o}{L_{o1}}(t - t_0), \tag{5}$$

$$i_{L_c}(t) = \left\{i_{pri}(t) - i_{L_{o1}}(t)\right\} \frac{L_{o2}}{L_{o2}+L_c}, \tag{6}$$

$$i_{L_{o2}}(t) = \frac{L_c}{L_{o2}+L_c} i_{pri}(t) + \frac{L_{o2}}{L_{o2}+L_c} i_{Lo1}(t), \tag{7}$$

where $\omega = 2\pi f_r = 1/\sqrt{\frac{L_{o2}L_c}{L_{o2}+L_c} C_r}$, $V_R = V_{in} - \frac{N_p}{N_s} V_{in}\left(1 + \frac{L_{o2}}{L_{o2}+L_c}\right)$.

Assuming that f_{sw} is equal to f_r, the following relationship is satisfied according to Kirchhoff's voltage law (KVL):

$$\frac{N_p}{N_s} = \frac{V_{in}}{2V_o\left(1 + \frac{L_{o2}}{L_{o2}+L_c}\right)} = \frac{V_{in}}{2V_o\left(1 + \frac{L_o}{L_o+L_c}\right)} \tag{8}$$

Here, (8) can be utilized in the design of the transformer turn ratio. When i_{pri} equals i_{Lo1} after resonance, this mode ends.

Mode 2 (t_1 - t_2): When i_{pri} equals i_{Lo1}, D_{o1} is blocked, and M_1 is turned off. Therefore, L_{o1} and L_{o2} are connected in series and resonate with C_r, as shown in Fig. 4(b). However, since t_1 - t_2 is very short from the assumption, $i_{pri} = i_{Lo1} = i_{Lo2}$ can be considered as a constant current source during this mode. Therefore, i_{pri} starts to charge C_{ds1} from 0 V to V_{in} and discharges C_{ds2} from V_{in} to 0 V. When v_{ds2} equals 0 V at t_2, M_2 can be turned on, with ZVS in the next mode.

Mode 3 (t_2-t_3): When M_2 is turned on, i_{pri} flows to the nondot terminal of the transformer, as shown in Fig. 4(c). Therefore, D_{o1} is blocked and the input power is transferred to the output through D_{o2}. Unlike the mode 1, the reflected voltage $(N_{p2}/N_{s2})V_o$ is applied to the winding N_{p2} of the second ideal transformer; thus, the series-connected L_c and $(N_{p2}/N_{s2})V_o$ are connected in parallel to L_{o1} through the first ideal transformer with the turn ratio of N_{p1}:N_{p1}. Then, the circuit inside the dashed box on the left side in Fig. 5(b) can be simplified to Thevenin's equivalent circuit, comprising a voltage source $(N_{p2}/N_{s2})V_oL_{o1}/(L_{o1} + L_c)$ and inductor $L_{o1}||L_c$, as shown on the right side in Fig. 5(b). In the equivalent circuit, N_{p2} and N_{s2} work as a transformer, whereas $L_{o1}||L_c$ acts as a resonant inductor. Therefore, i_{Lo2} is increased linearly with the slope of $(N_{p2}/N_{s2})V_o/L_{o2}$, and $L_{o1}||L_c$ resonates with C_r. Here, the currents and voltages are determined as follows:

$$i_{pri}(t) = \frac{N_p V_o T_s}{N_s 4 L_{o2}} \cos(\omega t) - \frac{\pi V_o I_o}{V_{in}} \sin(\omega t), \tag{9}$$

$$v_{C_r}(t) = V_R - \frac{N_p V_o T_s}{N_s 4 C_r \omega L_{o2}} \sin(\omega t) - \frac{V_o I_o T_s}{2 C_r V_{in}} \cos(\omega t), \tag{10}$$

$$i_{L_{o2}}(t) = \frac{N_p V_o T_s}{N_s 4 L_{o2}} - \frac{N_p}{N_s}\frac{V_o}{L_{o1}}(t - t_2), \tag{11}$$

$$i_{L_c}(t) = \{i_{pri}(t) - i_{Lo2}(t)\}\frac{L_{o1}}{L_{o1}+L_c}, \tag{12}$$

$$i_{L_{o1}}(t) = \frac{L_c}{L_{o1}+L_c} i_{pri}(t) + \frac{L_{o1}}{L_{o1}+L_c} i_{Lo2}(t), \tag{13}$$

where $\omega = 2\pi f_r = 1/\sqrt{\frac{L_{o1}L_c}{L_{o1}+L_c}C_r}$, $V_R = V_{in} - \frac{N_p}{N_s}V_{in}\left(1 + \frac{L_{o1}}{L_{o1}+L_c}\right)$.

Meanwhile, considering the same assumption at mode 1, the following relationship is also satisfied according to KVL:

$$\frac{N_p}{N_s} = \frac{V_{in}}{2V_o\left(1 + \frac{L_{o1}}{L_{o1}+L_c}\right)} = \frac{V_{in}}{2V_o\left(1 + \frac{L_o}{L_o+L_c}\right)}. \tag{14}$$

When i_{pri} equals i_{Lo2} after resonance, this mode ends.

Mode 4 (t_3 - t_4): When i_{pri} equals i_{Lo2}, D_{o2} is blocked and M_2 is turned off. Therefore, L_{o1} and L_{o2} are connected in series and resonate with C_r, as shown in Fig. 4(d). However, since t_3 - t_4 is very short, from the earlier assumption, $i_{pri} = i_{Lo1} = i_{Lo2}$ can be considered as a constant current source during this mode. Therefore, i_{pri} starts to charge C_{ds2} from 0 V to V_{in} and discharges C_{ds1} from V_{in} to 0 V. When v_{ds1} equals 0 V at t_4, M_1 can be turned on, with ZVS in following mode. From the abovementioned operations, whereas L_{o1} works as a magnetizing inductor and $L_{o2}||L_c$ acts as a resonant inductor at mode 1, $L_{o1}||L_c$ operates as a resonant inductor, and L_{o2} functions as a magnetizing inductor at mode 3. As a result, since the separated primary wire alternately operates as a transformer and an inductor, any external inductor or additional wires are unnecessary.

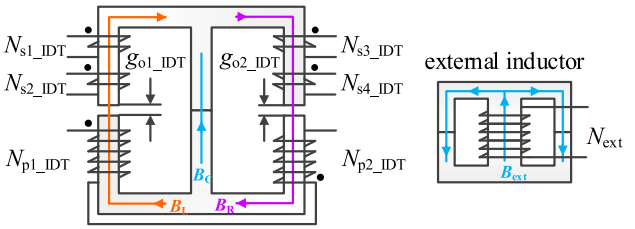

FIGURE 6. Magnetic structures of the IDT and external inductor.

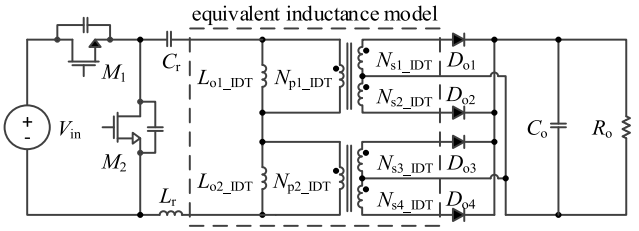

FIGURE 7. LRC configured with the equivalent inductance model of the IDT and external inductor.

C. EQUIVALENT PARAMETERS OF THE CONVENTIONAL IDT AND PROPOSED IMTP

Fig. 6 shows the magnetic structure of the conventional IDT, and Fig. 7 presents the LRC configured with the equivalent inductance model of the IDT, where $g_{o1\_IDT} = g_{o2\_IDT} = g_{o\_IDT}$, $L_{o1\_IDT} = L_{o2\_IDT} = L_{o\_IDT}$, $N_{p1\_IDT} = N_{p2\_IDT} = N_{p\_IDT}$, and N_{s1_IDT} - $N_{s4\_IDT} = N_{s\_IDT}$. In the IDT, the number of primary turns is split into half in each side leg; thus, the height of the transformer can be decreased, and the power density can be improved [10]. As shown in Fig. 6, each winding on the side leg is decoupled by the center leg of the core, and its wire connection is configured with series-input and parallel-output. Thus, the equivalent magnetizing inductance and turn ratio become $L_m = 2L_{o\_IDT}$ and $n_{eq} = 2N_{p\_IDT}$:N_{s_IDT}, respectively. However, if the IDT is implemented using a planar transformer to achieve a lower profile, its leakage inductance is too small to be used as a resonant inductor. Thus, an additional external inductor must be employed. However, the IMPT requires no additional inductor because $L_o||L_c$ of the IMPT acts as a resonant inductor ($L_r = L_o||L_c$).

Meanwhile, while the equivalent turn ratio of the IDT is determined as $n_{eq} = 2N_{p\_IDT}/N_{s\_IDT}$, and that of the IMPT is $n_{eq} = (N_p/N_s)\{1 + L_o/(L_o + L_c)\}$. Namely, the turn ratio of the IMPT can be roughly set to N_p/N_s and finely tuned by

$L_o/(L_o + L_c)$. For example, assuming that $V_{in(max)} = 390$ V and $V_o = 20.5$ V, the required turn ratio of the IDT should be $0.5\ V_{in(max)}/V_o{:}1 = 9.5{:}1$ to ensure operation at $f_{sw} = f_r$. Thus, since the number of turns must be an integer, the IDT should have $N_s = 4\,k$ [turns] and $N_p = 19\,k$ [turns] ($k = 1, 2, 3\ldots$). Consequently, the number of turns and core size of the IDT may become larger, regardless of the handled power.

However, in the proposed IMPT, various turn ratios can be implemented using L_o and L_c. Namely, when $N_s = k$ [turns] ($k = 1, 2, 3\ldots$), the turn ratio can be set precisely to 9.5:1 by setting $N_p = m$ [turns] (m = an integer greater than or equal to 9.5 k/2) and adjusting L_o and L_c to $(N_p/N_s)\{1 + L_o/(L_o + L_c)\} = 9.5$. Therefore, the proposed IMPT can have as many turns as required, and its size can be optimally designed in any input/output (I/O) specifications.

Meanwhile, the following relationship from (14) should be satisfied to make the same voltage conversion ratios of the traditional single transformer (TST) and the proposed IMPT equal to each other:

$$n_{eq} = \frac{V_{in}/2}{V_o} = \frac{N_p}{N_s}\left(1 + \frac{L_o}{L_o + L_c}\right). \tag{15}$$

Moreover, since the current slope of the magnetizing inductor also should be the same as the TST, following relationship should also be satisfied.

$$\frac{n_{eq}V_o}{L_m} = \frac{N_{p1}}{N_{s1}}\frac{V_o}{L_{o1}} = \frac{N_p}{N_s}\frac{V_o}{L_o} \tag{16}$$

Therefore, the equivalent magnetizing inductor of the proposed IMPT is represented by $L_o\{1 + L_o/(L_o + L_c)\}$. As a result, the equivalent parameters of the TST, conventional IDT, and proposed IMPT can be summarized in Table 1.

TABLE 1. Comparison of equivalent parameters.

Parameters	TST	IDT	IMPT
Magnetizing inductor	L_m	$2L_{o\_IDT}$	$L_o\left(1 + \frac{L_o}{L_o + L_c}\right)$
Resonant inductor	L_r	External Inductor	$L_o \parallel L_c$
Turn ratio	n_{eq}	$2\frac{N_{p\_DT}}{N_{s\_DT}}$	$\frac{N_p}{N_s}\left(1 + \frac{L_o}{L_o + L_c}\right)$

III. DESIGN CONSIDERATIONS

A. TURN RATIO OF THE IMPT

In the mode analysis, the turn ratio of the IMPT was determined as (8) and (14). By defining the ratio of L_o and L_r as L_n ($= L_o/L_r = L_o/(L_o||L_c)$), the turn ratio can be expressed again as follows:

$$\frac{N_p}{N_s} = \frac{V_{in(max)}}{2V_o\left(1 + \frac{L_o}{L_o + L_c}\right)} = \frac{V_{in(max)}}{2V_o\left(2 - \frac{1}{L_n}\right)}, \tag{17}$$

where the turn ratio is determined by L_n.

As L_o and L_c are always greater than 0, $L_o/(L_o + L_c)$ in (17) has a value between 0 and 1. Thus, the range of the turn ratio is considered to be $0.5V_{in(max)}/V_o$ to $0.25V_{in(max)}/V_o$.

B. VOLTAGE GAIN OF THE PORPOSED IMPT LRC

Using the equivalent parameters described in Table 1, the IMPT LRC can be converted into the equivalent TST LRC. Therefore, the voltage gain of the IMPT LRC can be derived by performing the same process as the TST LRC. Assuming that the fundamental components of all alternating voltages and currents in the LRC are dominant, the I/O voltage gain $H(s)$ can be easily obtained using the fundamental harmonic approximation (FHA) as follows [20], (18) as shown at the bottom of the next page, where $L_{neq} = L_m/L_r = 2L_n - 1$, $F = f_{sw}/f_r$, $f_r = 1/\left(2\pi\sqrt{L_r/C_r}\right)$, $Q_e = R_{eq}/\sqrt{L_r/C_r}$, $R_{eq} = n^2\sqrt{8/\pi^2}\frac{V_o}{I_o}$, $\omega_r = 2\pi f_r$, and $n_{eq} = n\{1 + L_o/(L_o + L_c)\}$.

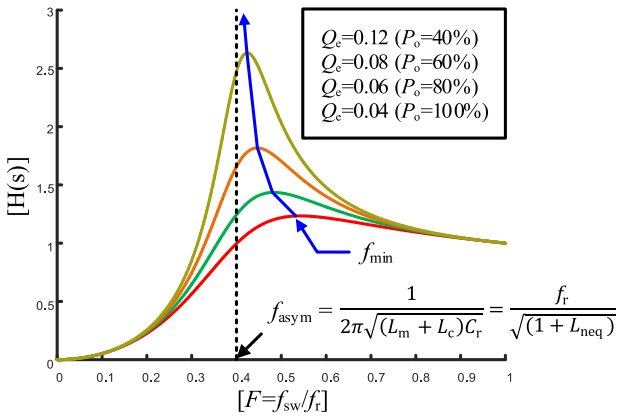

FIGURE 8. Voltage gain as a function of Q_e ($V_{in(max)} = 390$ V, $V_o = 19.5$ V, $P_o = 350$ W, $L_r = 5.9$ uH, $C_r = 6.6$ nF, $f_r = 800$ kHz, $L_{neq} = 5$, and $N_{eq} = 10$).

Based on (18), the $H(s)$ is a function of the normalized switching frequency, and Q_e is shown in Fig. 8. The Fig. 8 indicates that as Q_e increases, the minimum switching frequency f_{min} for peak voltage gain approaches the asymptotic frequency f_{asym}, which is determined by $L_m + L_r$ and C_r [5], [20]. Since the voltage gain at f_{asym} is not only always lower than at f_{min} but also similar to each other, the f_{min} that guarantees the required peak voltage gain can be assumed to be equal to f_{asym} as follows:

$$f_{min} \cong f_{asym} = \frac{1}{2\pi\sqrt{(L_m + L_r)\,C_r}} = \frac{f_r}{\sqrt{1 + L_{neq}}} = \frac{f_r}{\sqrt{2L_n - 1}}. \tag{19}$$

To ensure the required peak $H(s)$ at the minimum input voltage $V_{in(min)}$, the converter is operated in f_{min} and $F_{min} = f_{min}/f_r$. Thus, the range of L_o can be determined from (16) and (17) as follows, (20) as shown at the bottom of the next page.

In addition, L_r and C_r can be determined from the relationship among L_o, L_n, and f_r as follows:

$$L_r = \frac{L_o}{L_n} = \frac{L_o L_c}{L_o + L_c}, \tag{21}$$

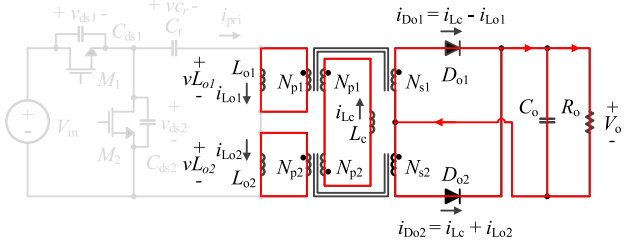

FIGURE 9. Mode 1 operation at $v_{cr} = V_{in}$ (t_0 - t_1).

$$L_c = \frac{L_o L_r}{L_o - L_r}, \tag{22}$$

$$C_r = \frac{1}{4\pi^2 f_r^2 L_r}. \tag{23}$$

From (20), (21), and (23), the range of C_r that ensures the required peak voltage gain can be determined as follows:

$$C_r \geq \frac{\pi V_o \left| F_{min} - \frac{1}{F_{min}} \right|}{8 f_r V_{inmin} n R_o \sqrt{\left| 1 - \left(\frac{2nV_o}{V_{inmin}} \right)^2 \left\{ 1 + \frac{1}{2L_n - 1} \left(1 - \frac{1}{F_{min}^2} \right) \right\}^2 \right|}} \tag{24}$$

C. RESONANT CAPACITOR FOR ENSURING NORMAL OPERATION

As described in Section II-B, D_{o2} is turned off and the input power is transferred to the output through D_{o1} during mode 1 because i_{pri} flows to the dot terminal of the transformer. At the same time, v_{cr} increases while v_{Lo2} decreases according to v_{cr}. However, if v_{cr} exceeds V_{in} at t_A in Fig. 10, v_{Lo1} and v_{Lo2} become nV_o and $-nV_o$, respectively. Then, v_{cr} is clamped on V_{in}. Thus, as shown in Figs. 9 and 10, i_{pri} becomes 0 A during t_A - t_B, and i_{Do1} and i_{Do2} flow through D_{o1} and D_{o2} as follows:

$$i_{Do1}(t) = \frac{N_p}{N_s} \left(i_{Lc}(t) - i_{Lo1}(t) \right), \tag{25}$$

$$i_{Do2}(t) = \frac{N_p}{N_s} \left(i_{Lc}(t) + i_{Lo2}(t) \right), \tag{26}$$

The fact that i_{pri} equals 0 A indicates that the I/O voltage gain is reduced because the input power is not transferred to the output. To overcome this problem and guarantee normal

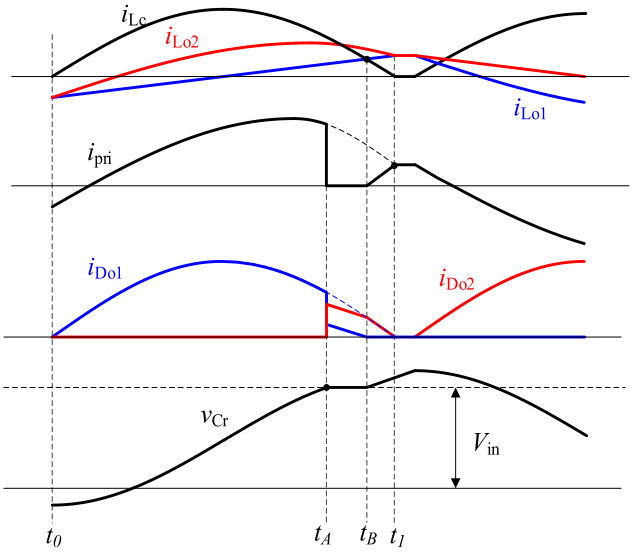

FIGURE 10. Key waveforms at $v_{cr} = V_{in}$ in mode 1 (t_0 - t_1).

operation for the IMPT, v_{cr} should be kept lower than V_{in} until the resonance is over.

Meanwhile, the peak value of v_{cr} occurs when $V_{in} = V_{in(min)}$ and $f_{sw} = f_{min}$. Considering the FHA mentioned in Section III-B, the peak value of v_{cr} can be easily obtained from (4). Therefore, the C_r that guarantees the normal operation can be obtained as follows:

$$C_r > \frac{P_o}{f_{min} V_{in(min)}^2 \sqrt{\left| 1 - \left(\frac{\pi}{4L_n - 2} \right)^2 \right|}} \tag{27}$$

The value of C_r affects normal operation as well as the I/O voltage gain of the IMPT. Therefore, C_r should be selected by considering (24) for the maximum required voltage gain and (27) for normal operation. For example, assuming that $V_{in(max)} = 390$ V, $V_{in(min)} = 320$ V, $V_o = 19.5$ V, and $P_o = 350$ W, the available range of turn ratio can be obtained from (17) as $5 < N_p/N_s < 10$. Considering the available turn ratio, the range of C_r as a function of N_p/N_s and f_r is shown in Fig. 11. It can be observed that overlapping areas represent the available values for C_r which satisfy both the required peak voltage gain and the normal operation.

$$H(s) = \frac{2n_{eq}V_o}{V_{in}} = \frac{1}{\sqrt{\left\{ 1 + 1/L_{neq}(1 - 1/F^2) \right\}^2 + \left\{ 1/Q_e(F - 1/F) \right\}^2}} \tag{18}$$

$$L_o \leq \frac{2L_n V_{in(min)} n_{eq} R_o}{\pi^3 f_r V_o \left| F_{min} - \frac{1}{F_{min}} \right| \sqrt{\left| 1 - \left(\frac{2n_{eq}V_o}{V_{in(min)}} \right)^2 \left\{ 1 + \frac{1}{2L_n - 1} \left(1 - \frac{1}{F_{min}^2} \right) \right\}^2 \right|}}. \tag{20}$$

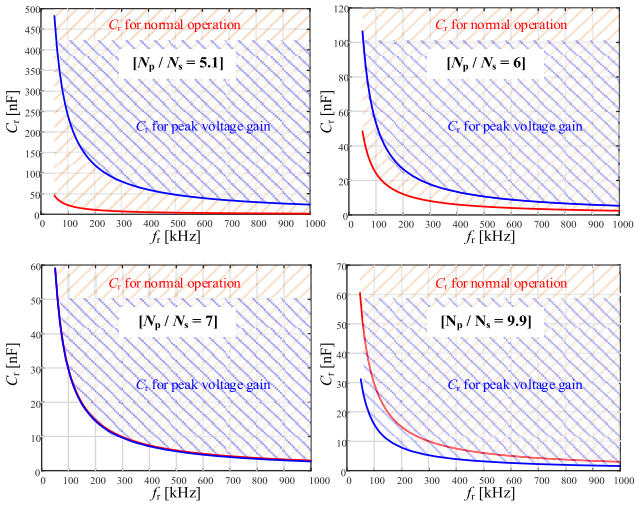

FIGURE 11. Range of C_r as a function of N_p/N_s and f_r.

Meanwhile, the larger turn ratio requires smaller L_o and L_c from (17); thus, the circulating current and current stress may be increased. Furthermore, the number of turns and layers in the planar transformer are also increased. Therefore, these points should be considered when designing circuit parameters. Finally, the appropriate resonant frequency should be selected to achieve the highest efficiency through loss analysis, which is considered later.

IV. OPTIMAL PARAMETERS DETERMINATION

A. LOSS ANALYSIS FOR THE OPTIMAL PARAMETERS

The overall efficiency of the converter is mainly determined by critical components, such as the main switches, magnetic devices, and output rectifiers. Since the main switch is turned on under the ZVS condition, its turn-on switching loss can be ignored. In the output rectifier, the synchronous rectifier FET is generally used instead of a diode to reduce the conduction loss in high-current applications.

In magnetic devices, power losses are divided into core and copper loss. The core loss is greatly affected by magnetic materials at high frequency as high as 800 kHz. Thus, the core loss densities at 800 kHz of four different magnetic materials as a function of the flux density are shown in Fig. 12. Here, the ML90S exhibits the lowest core loss.

Meanwhile, in the copper loss, it is also greatly affected by the AC resistance of the conductor at high frequency. Therefore, the thickness of the layer in the planar transformer should be optimally designed to minimize the copper loss caused by the effective resistance. From [21], the effective resistance is given by:

$$R_{dc} = \rho \frac{N \cdot MLT}{A_c} [\Omega], \tag{28}$$

$$R_{eff} = R_{dc} \left\{ 1 + \frac{\Psi}{3} \Delta^4 \left(\frac{i'_{rms}}{\omega_r i_{rms}} \right)^2 \right\} [\Omega]. \tag{29}$$

Based on the abovementioned points, the loss analysis equations are summarized in Table 2. In this table,

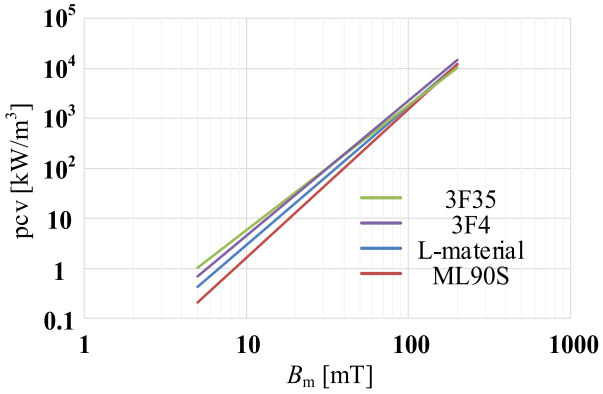

FIGURE 12. Core loss density as a function of flux density of different core materials at 800 kHz.

t_f and $R_{ds(on)}$ are the FET turn-off time and turn-on resistance, and V_e is the volume of the magnetic core. Additionally, the core loss coefficients of ML90S and the key currents equations are given in Tables 3 and 4, respectively.

Meanwhile, performance and efficiency of the LRC are greatly affected by resonant parameters. Thus, it is desirable to design the circuit parameters to have the highest efficiency within the range, ensuring a sufficient voltage gain and normal operation of the LRC.

For these reasons, based on the efficiency analysis according to the turn ratio and f_r, the design process of optimal circuit parameters is presented as follows. The efficiency analysis is performed under the I/O specifications in Section III-C ($V_{in(max)} = 390$ V, $V_o = 19.5$ V, $P_o = 350$ W) as an example. Moreover, f_{sw} is set equal to f_r to minimize circulating current and variation of f_{sw} according to load.

First, from the I/O voltage specifications, the range of turn ratio can be derived as $5 < N_p/N_s < 10$ by (17). Assuming that f_{sw} is high enough to ensure that the magnetic core is not saturated, the available number of turns to minimize the transformer size can be determined as follows. Considering the fact that the number of turns in the transformer should be an integer, the number of primary and secondary turns can be implemented as $N_p = 6T, 7T, 8T, 9T$, and $N_s = 1$. And, L_n in each case can also be determined from (17).

Next, the f_{min} according to the given f_r can be determined from (19), and the range of L_o to satisfy the enough voltage gain can also be derived from (20). At this point, it is desirable to select L_o as the maximum value within the range satisfying the voltage gain because lower L_o can cause the larger switching and conduction losses, listed in Table 2 to Table 4.

Finally, L_r, L_c, and C_r can be determined from (21) - (23), respectively. At this point, it must be checked whether C_r satisfies the conditions (24) and (27) to ensure the voltage gain and normal operation. If both conditions above are not met due to the small C_r, L_r, and L_c, then C_r should be reselected by reducing L_o.

Through the abovementioned process, Fig. 13 shows the power conversion efficiency according to the f_r and turn ratio. It can be observed that the highest efficiency can be achieved

TABLE 2. Equations for loss analysis.

Parameter		Equation
Switch	Turn off	$P_{\text{turn\_of}} = \frac{1}{2} t_f v_{ds} i_{Lo\_peak} f_{sw}$ [W]
	Conduction	$P_{\text{conduction}} = i_{sw\_rms}^2 R_{ds(on)}$ [W]
	C_{gs}	$P_{gs} = C_{gs} v_{gs}^2 f_{sw}$ [W]
Transformer	Core	$k B_m^{\alpha} f_{sw}^{\beta} V_e$ [W]
	Pattern	$R_{ef\_pri} i_{pri\_rms}^2 + R_{ef\_sec} i_{sec\_rms}^2$ [W]
Output Rectifier	Conduction	$2 R_{ds(on)} i_{sec\_rms}^2$ [W]
	C_{gs}	$P_{gs} = C_{gs} v_{gs}^2 f_{sw}$ [W]

TABLE 3. Material loss coefficients of ML90S.

material	temp.(°C)	k	α	β
ML90S	20	1.862E-04	2.857	1.667
	100	3.939E-04	2.972	1.958

TABLE 4. Key current equations.

Parameter		Equation
Transformer	i_{Lo_peak}	$\frac{N_p}{N_s}\frac{V_{in}}{4L_o}T_s$
	i_{pri_rms}	$\frac{1}{\sqrt{2}}\sqrt{\left(\frac{N_p}{N_s}\frac{V_o T_s}{4L_o}\right)^2 + \left(\frac{\pi P_o}{V_{in}}\right)^2}$
	i_{pri_rms}'	$\frac{\omega}{\sqrt{2}}\sqrt{\left(\frac{N_p}{N_s}\frac{V_o T_s}{4L_o}\right)^2 + \left(\frac{\pi P_o}{V_{in}}\right)^2}$
	i_{sec_rms}	$I_o\frac{\pi}{4}$
	i_{sec_rms}'	$I_o\frac{\omega\pi}{4}$
Switch	i_{sw_rms}	$\frac{1}{2}\sqrt{\left(\frac{N_p}{N_s}\frac{V_o T_s}{4L_o}\right)^2 + \left(\frac{\pi P_o}{V_{in}}\right)^2}$

in $N_p/N_s = 6, f_r = 800$ kHz, which is originated from the fact that rms currents in the circuit and total losses become small at the low turn ratio because lower turn ratio requires larger L_o. Therefore, the optimal parameters of the proposed IMPT LRC can be finally designed as N_p: N_s = 6:1, L_o = 18 uH, L_r = 5.9 uH, L_c = 8.9 uH, and C_r = 6.6 nF at f_r = 800 kHz. Additionally, the optimal thickness of the PCB layer can be determined to minimize copper losses. In Table 2, the copper loss of the planar transformer is affected by the rms currents and R_{eff} of the PCB. From (28) and (29), it can be observed that R_{eff} is mainly affected by the copper thickness, number of layers and switching frequency. Based on the determined parameters, the conduction losses of primary, secondary, and overall wires according to the copper thickness are calculated under full load conditions, as shown in Fig. 14.

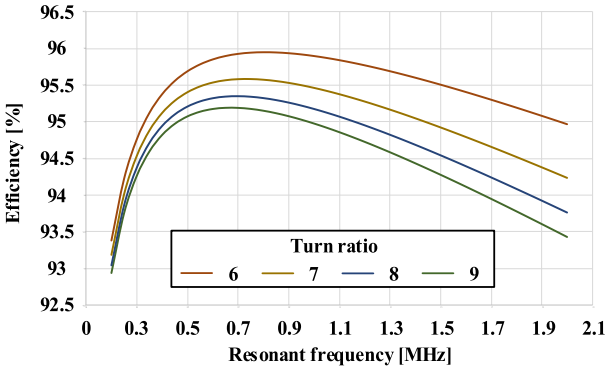

FIGURE 13. Power conversion efficiency according to the f_r and turn ratio.

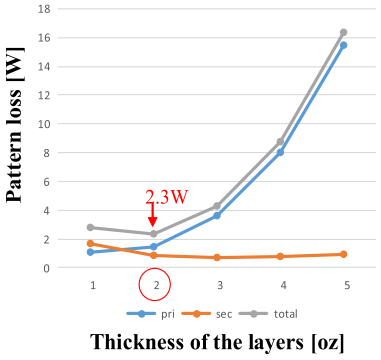

FIGURE 14. Calculated copper losses according to the thickness of the layer at f_{sw} = 800 kHz.

From these results, it can be observed that the 2 oz layer can minimize the total copper losses and it can be the optimum thickness of the layer at f_{sw} = 800kHz.

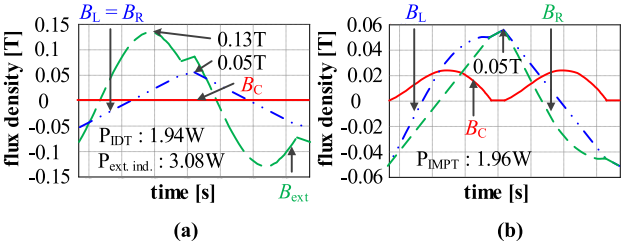

FIGURE 15. Magnetic flux density at V_{in} = 390 V, V_o = 19.5 V, and P_o = 350 W: (a) IDT with an external inductor (L_o = 15 uH, N_p: N_s = 5 : 1, L_r = 5.9 uH, and N_{ind} = 4), (b) IMPT (L_o = 18 uH, L_c = 8.9 uH, and N_p: N_s = 6 : 1).

B. COMPARISON BETWEEN IDT AND IMPT IN TERMS OF MAXIMUM FLUX DENSITY AND CORE LOSS

A comparison of the magnetic flux density between the IDT and IMPT is shown in Fig. 15. From the above determined parameters of IMPT, equivalent parameters of the IDT and IMPT can be derived from Table 1 as follows: L_m = 30 uH,

L_r = 5.9 uH, C_r = 6.6 nF, n_{eq} = 10, and f_r = 800 kHz. In addition, EE3112-ML90S (A_c = A_o = 128 mm^2) and EE1604-ML90S (A_c = 40.5 mm^2, A_o = 18 mm^2) are used as a transformer and external inductor core, respectively. As shown in Fig. 15(a), the IDT exhibits a flux density (B) of –0.05 T < B_L = B_R < 0.05 T in the side legs and a zero flux density in the center leg with the aid of flux cancellation. Consequently, the core loss is as low as 1.94 W.

Nevertheless, since the large resonant current flows directly through the external inductor L_r, where B is –0.13 T < B_{ext} < 0.13 T; thus, its core loss is as high as 3.08 W. Although the larger number of turns or a larger core are capable of reducing the core loss of the external inductor, more PCB layers are required, causing higher manufacturing costs or a significant reduction in the power density.

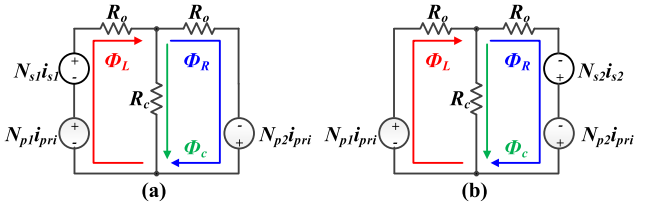

FIGURE 16. Equivalent reluctance model of the IMPT according to the key operations: (a) mode 1, (b) mode 3.

However, in the IMPT, the magnetic flux generated from the magnetizing current flows through one of the side legs, whereas the magnetic flux generated from the resonant current is divided into the side and center legs. From the reluctance model in Fig. 16, each magnetic flux can be determined as follows [22]–[25]:

$$\Phi_{L(mode1)} = \Phi_{R(mode3)} = \frac{\Re_o + \Re_c}{\Re_o^2 + 2\Re_o\Re_c}\left(N_{p1}i_{pri} + N_{s1}i_{s1}\right) + \frac{\Re_c}{\Re_o^2 + 2\Re_o\Re_c}N_{p2}i_{pri} \quad (30)$$

$$\Phi_{R(mode1)} = \Phi_{L(mode3)} = \frac{\Re_c}{\Re_o^2 + 2\Re_o\Re_c}\left(N_{p1}i_{pri} + N_{s1}i_{s1}\right) + \frac{\Re_o + \Re_c}{\Re_o^2 + 2\Re_o\Re_c}N_{p2}i_{pri} \quad (31)$$

$$\Phi_c = \frac{\Re_o}{\Re_o^2 + 2\Re_o\Re_c}\left(N_{p1}i_{pri} + N_{s1}i_{s1} - N_{p2}i_{pri}\right) \quad (32)$$

From (30) - (32), the IMPT exhibits a flux density of –0.05 T < B_L = B_R < 0.05 T in the side leg and 0 < B_C < 0.021 T in the center leg, as shown in Fig. 15 (b). Accordingly, since the flux density (B) in the side legs of the IMPT and IDT are almost identical; thus, their core losses are also the same. However, as B in the center leg of the IDT is zero, its core loss also becomes zero. Whereas in the IMPT, since the magnetic flux flows through the center leg, B is not zero and the resultant core loss exists. Nevertheless, the maximum magnetic flux density (B_m) in the center leg is not only low but the center leg also occupies a small fraction of the total core volume. Thus, the core loss of the IMPT is slightly larger than that of the IDT. However, both are approximately the same, as shown in Fig. 17.

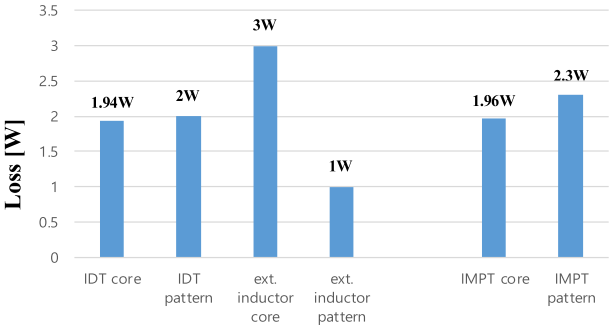

FIGURE 17. Magnetic loss comparison between the IMPT and IDT at f_{sw} = 800 kHz.

Meanwhile, as described in Table 1, the IDT and IMPT have different turn ratios, but their equivalent turn ratios n_{eq} can be exactly the same. Therefore, the copper loss of the IMPT is slightly higher than that of the IDT as shown in Fig. 17, because the IMPT has two more turns than the IDT. Nevertheless, since the additional losses caused by the external inductor can further degrade the efficiency of the IDT LRC, as shown in Fig. 17; therefore, the IMPT is more advantageous in terms of overall system efficiency and size. As a result, the IMPT can be an excellent solution for high power density and high efficiency in the LRC.

C. INDUCTANCE MEASUREMENT METHOD OF THE IMPT

In order to ensure the input-to-output voltage conversion ratio and stable resonant operation in the TST LRC, the magnetizing inductor L_m and resonant inductor L_r should be appropriately designed. Likewise, to implement the equivalent L_m and L_r in the IMPT LRC, L_o and L_c should be appropriately designed according to equivalent parameters presented in Table 1. Therefore, the inductance measurement method of the IMPT is presented, as shown in Fig. 18.

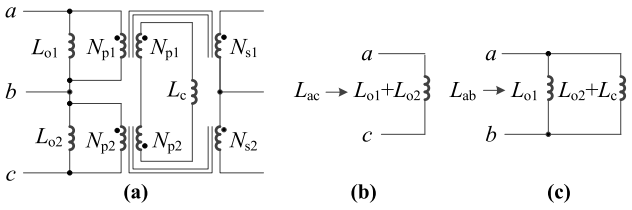

FIGURE 18. Inductance measurement method of the IMPT: (a) equivalent inductance model of the IMPT (b) simplified circuit of L_{ac} (c) simplified circuit of L_{ab}.

First, the primary inductance L_{ac} is measured between nodes a and c with the secondary side open. If it is assumed that N_{p1} = N_{p2} = N_p and L_{o1} = L_{o2} = L_o, the voltage across L_c always becomes zero due to the same voltage and opposite polarity of N_{p1} and N_{p2}. Therefore, L_c can be neglected and

the equivalent inductance between nodes a and c is equal to the series-connected L_{o1} and L_{o2}, as shown in Fig. 18(b). Namely, L_{ac} is equal to $L_{o1} + L_{o2} = 2L_o$; thus, L_o can be expressed as follow:

$$L_o = \frac{L_{ac}}{2}. \tag{33}$$

Second, the half primary inductance L_{ab} is measured between nodes a and b with the other half primary side (between nodes b and c) and secondary side open. In Fig. 18(a), L_{o2} is connected in series with L_c through the second ideal transformer with a turn ratio of N_{p2}: N_{p2}. At the same time, series-connected L_{o2} and L_c are again connected in parallel to L_{o1} through the first ideal transformer with the turn ratio of N_{p1}: N_{p1} as shown in Fig. 18(c). Therefore, L_{ac} is equal to $L_{o1}//(L_{o2} + L_c) = L_o//(L_o + L_c)$; thus, L_c can be expressed as follow:

$$L_c = \frac{2L_{ab}{}^2 L_o - L_o^2}{L_o - L_{ab}}. \tag{34}$$

In summary, the equivalent inductances L_o and L_c can be obtained by measuring the inductances L_{ac} and L_{ab} among nodes a, b and c.

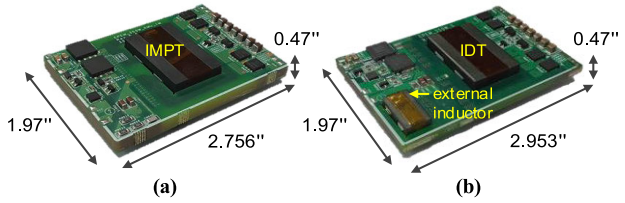

FIGURE 19. 350 W LRC prototypes: (a) configured with the proposed IMPT, (b) configured with the IDT.

V. EXPERIMENTAL RESULTS BASED ON OPTIMAL DESIGN

The 350W - LRC prototypes equipped with the IDT and IMPT are shown in Fig. 19. The IMPT allows the LRC to operate without an external inductor. Therefore, the power density of the IMPT LRC can be improved by approximately 7.15% compared to the IDT LRC and by up to 137.16 W/in^3.

The I/O specifications and parameters used in the experiment are listed in Table 5. To achieve the high efficiency and low heat generation of the high switching frequency and high power density converter, 600 V GaN-FETs and 80 V Si-FETs with low turn-on resistance are used as primary side power switches and secondary side Synchronous Rectifiers respectively. Table 6. lists the specifications of power switches used in the prototype.

Figs. 20 (a) - (c) present the experimental key waveforms of the IMPT LRC according to the load conditions. These prove that the IMPT LRC operates in exactly the same way as the conventional LRC. In addition, M_2 is turned on after v_{ds2} becomes 0 V (i.e. the ZVS of M_2 is achieved for the entire load range).

TABLE 5. Parameters used in the experiment.

Parameter	Value		Unit
	IDT	IMPT	
Input voltage V_{in}	320 ~ 390		V_{DC}
Output voltage V_o	19.5		V_{DC}
Output power P_{o_max} / P_{o_typ}	350 / 200		W
Resonant capacitance C_r	6.6		nF
Side leg inductance	L_{o_IDT} = 15	L_o = 18	uH
Center leg inductance	-	L_c = 8.9	uH
Equivalent magnetizing inductance L_m	30		uH
Equivalent resonant inductance L_r	5.9		uH
Equivalent Turn ratio n_{eq}	10:1		
Transformer : Number of turns	N_{p_IDT} = 5 N_{s_IDT} = 1	N_p = 6 N_s = 1	Turns
Resonant frequency f_r	800		kHz

TABLE 6. Specifications of power switches used in prototype.

Parameters	Value		Unit
	TPH3206PD (GaN-FET)	BSC061N08NS5 (Si-FET)	
Breakdown voltage	600	80	V
Turn-on resistance	0.18	0.0061	Ohm
Input capacitance	760	2000	pF
Output capacitance	44	300	pF
Rise / Fall time	4.5 / 4	6 / 5	ns

Since M_1 operates exactly symmetrically with M_2, the ZVS of M_1 can also be achieved (corresponding waveforms are not presented here). The voltage gain for the input voltage range is verified by the key experimental waveforms in Fig. 20 (d) at V_{in} = 320 V and a full load, proving that the converter can regulate the output voltage at 19.5V under minimum input voltage condition with sufficient voltage gain.

Fig. 21 shows the experimental key waveforms of the IDT LRC at full load condition. As shown in this figure, it can be observed that the IDT LRC and IMPT LRC work almost identically and have almost the same switching frequency because they have the same equivalent resonant parameters, as shown in Table 5.

Here, the operation of the IDT LRC is exactly the same as the TST LRC because the sum of the magnetizing inductor in the IDT is revealed as that in a single transformer ($L_{o1\_IDT} + L_{o2\_IDT} = L_m$). Therefore, corresponding waveforms of the TST LRC are omitted in this paper.

Fig. 22 shows the experimental key waveforms in dynamic load transients of the IMPT LRC, where the load is changed from a typical (200 W) load to no-load with a 6-msec period and 50% duty cycle. As shown in Fig. 22, the output voltage is well regulated within 5% while the load is changed, and the switching frequency is changed narrowly from 775kHz to 794kHz. These results prove that the IMPT has good output voltage regulation and load transient performance without an external inductor.

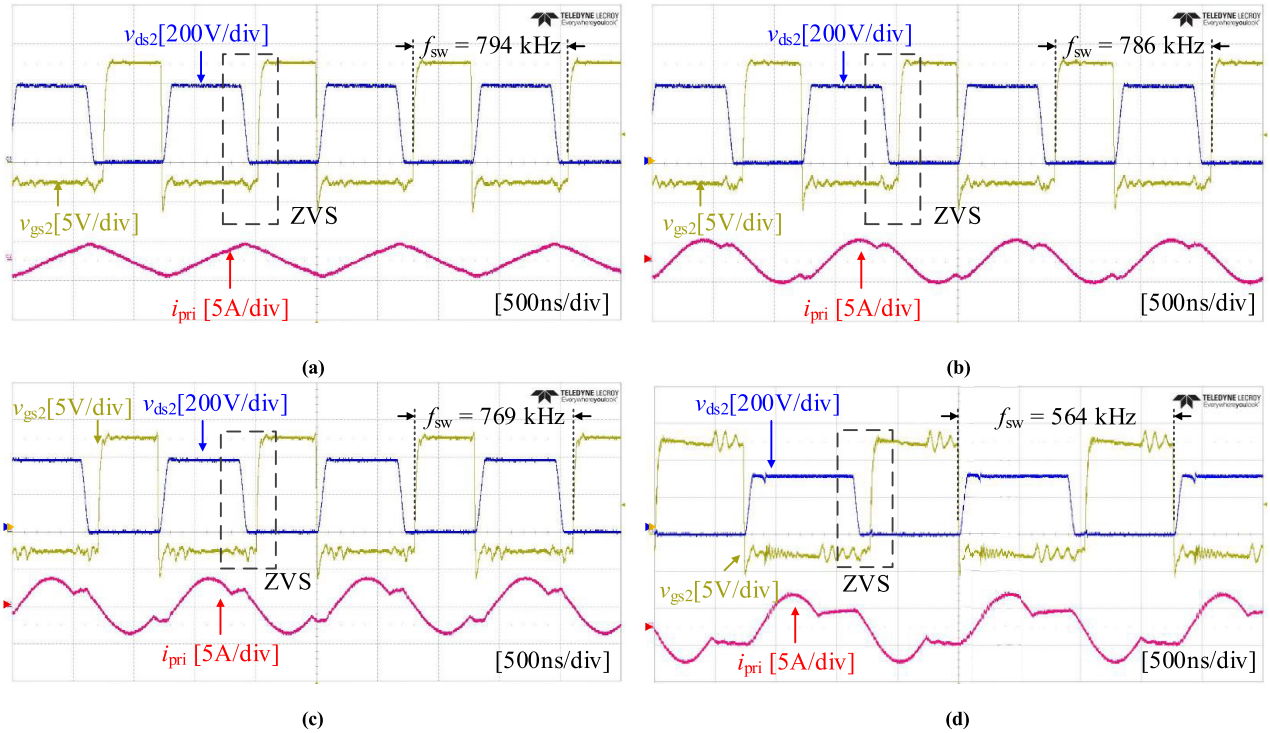

FIGURE 20. Experimental key waveforms of the 350 W IMPT LRC: (a) V_{in} = 390 V, I_o = no load, (b) V_{in} = 390 V, I_o = half load, (c) V_{in} = 390 V, I_o = full load, (d) V_{in} = 320 V, I_o = full load.

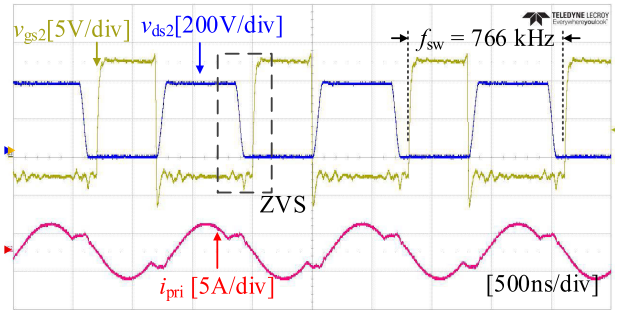

FIGURE 21. Key waveforms of the 350 W IDT LRC at full load.

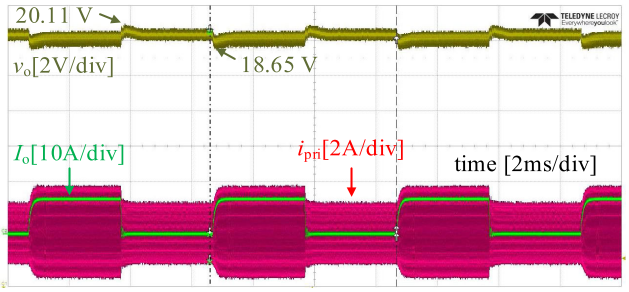

FIGURE 22. Key waveforms in load transient (P_{o_typ} → no load).

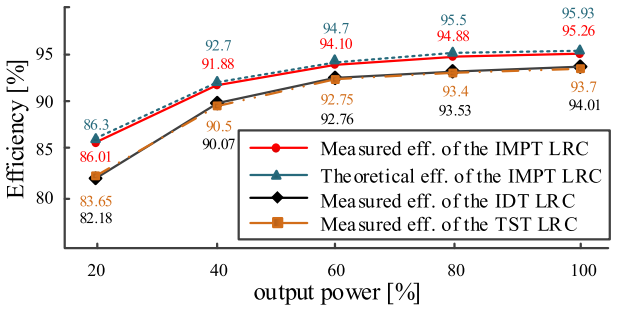

FIGURE 23. Efficiency comparisons according to the output power.

The theoretical and measured efficiency of the IMPT LRC is presented in Fig. 23. The measured efficiency of the IDT LRC and TST LRC are also presented for comparison. These results prove that the theoretical efficiency of the IMPT LRC is almost equivalent to the measured efficiency, confirming the validity of the theoretical analysis.

The measured efficiency of the IMPT LRC is more than 91.88% under conditions of 40% or more load, and the maximum efficiency is measured up to 95.26% at a full load condition. However, the efficiency is somewhat low at a light load because the operating frequency is as high as about 800 kHz.

Meanwhile, the IMPT has a higher efficiency than that of the IDT and TST through the entire load range.

This difference in efficiency is originated from the fact that the IMPT does not require a separate external inductor.

VI. CONCLUSION

In this paper, an IMPT for a high efficiency and high power density LRC is proposed. In the proposed methodology, the primary wire is split into each side leg of the EE-type magnetic core, and each operates as a transformer and inductor alternatively in every switching period. Therefore,

a low-profile single planar transformer can be implemented without the need of an external inductor or additional wires. Moreover, since the magnetic flux density of the proposed IMPT is similar to that of a conventional transformer; thus, the same size core can be implemented. As a result, further losses from the external inductor are saved. Therefore, with a single planar transformer, the IMPT can achieve higher efficiency and power density than with a conventional transformer.

The operation of the LRC configured with the IMPT was verified by an equivalent inductance model, providing detailed design considerations. Based on the loss analysis comparison with that of a conventional transformer, improved performance of the IMPT was verified by the experimental results of the 350 W prototypes. These results confirm that the IMPT can operate exactly the same as the LRC without an extra inductor or additional wires. In addition, the comparisons of the measured and theoretical efficiency indicate the reliability of the design considerations and magnetic analysis. From these results, the IMPT is suitable for various LRC applications that require high power density and high efficiency.

REFERENCES

[1] B. Lu, W. Liu, Y. Liang, F. C. Lee, and J. D. van Wyk, "Optimal design methodology for LLC resonant converter," in *Proc. 21st Annu. IEEE Appl. Power Electron. Conf. Expo. (APEC)*, Dallas, TX, USA, Mar. 2006, pp. 533–538.

[2] S. Ji, D. Reusch, and F. C. Lee, "High-frequency high power density 3-D integrated gallium-nitride-based point of load module design," *IEEE Trans. Power Electron.*, vol. 28, no. 9, pp. 4216–4226, Sep. 2013.

[3] X. Huang, Z. Liu, Q. Li, and F. C. Lee, "Evaluation and application of 600 V GaN HEMT in cascode structure," *IEEE Trans. Power Electron.*, vol. 29, no. 5, pp. 2453–2461, May 2014.

[4] R. Chen, P. Brohlin, and D. Dapkus, "Design and magnetics optimization of LLC resonant converter with GaN," in *Proc. IEEE Appl. Power Electron. Conf. Expo. (APEC)*, Tampa, FL, USA, Mar. 2017, pp. 94–98.

[5] B. Yang, F. C. Lee, A. J. Zhang, and G. Huang, "LLC resonant converter for front end DC/DC conversion," in *Proc. 17th Annu. IEEE Appl. Power Electron. Conf. Expo. (APEC)*, Dallas, TX, USA, Mar. 2002, pp. 1108–1112.

[6] D. Fu, B. Lu, and F. C. Lee, "1 MHz high efficiency LLC resonant converters with synchronous rectifier," in *Proc. IEEE Power Electron. Spec. Conf.*, Jun. 2007, Orlando, FL, USA, pp. 2404–2410.

[7] D. Reusch and F. C. Lee, "High frequency bus converter with low loss integrated matrix transformer," in *Proc. 27th Annu. IEEE Appl. Power Electron. Conf. Expo. (APEC)*, Orlando, FL, USA, Feb. 2012, pp. 1392–1397.

[8] D. Huang, S. Ji, and F. C. Lee, "LLC resonant converter with matrix transformer," *IEEE Trans. Power Electron.*, vol. 29, no. 8, pp. 4339–4347, Aug. 2014.

[9] M. Mu and F. C. Lee, "Design and optimization of a 380–12 V high-frequency, high-current LLC converter with GaN devices and planar matrix transformers," *IEEE J. Emerg. Sel. Topics Power Electron.*, vol. 4, no. 3, pp. 854–862, Sep. 2016.

[10] S. Iqbal, "Interleaved LLC resonant converter with integrated dual transformer for PV power systems," in *Proc. 8th IET Int. Conf. Power Electron., Mach. Drives (PEMD)*, Glasgow, U.K., 2016, pp. 1–6.

[11] W. Chen, G. Hua, D. Sable, and F. Lee, "Design of high efficiency, low profile, low voltage converter with integrated magnetics," in *Proc. Appl. Power Electron. Conf. (APEC)*, Atlanta, GA, USA, 1997, pp. 911–917.

[12] S. Gao and Z. Zhao, "Magnetic integrated LLC resonant converter based on independent inductance winding," *IEEE Access*, vol. 9, pp. 660–672, 2021.

[13] P. He, A. Mallik, G. Cooke, and A. Khaligh, "High-power-density high-efficiency LLC converter with an adjustable-leakage-inductance planar transformer for data centers," *IET Power Electron.*, vol. 12, no. 2, pp. 303–310, Feb. 2019.

[14] B. Yang, R. Chen, and F. C. Lee, "Integrated magnetic for LLC resonant converter," in *Proc.17th Annu. IEEE Appl. Power Electron. Conf. Expo.*, Dallas, TX, USA, Mar. 2002, pp. 346–351.

[15] Y. Zhang, D. Xu, K. Mino, and K. Sasagawa, "1 MHz–1 kW LLC resonant converter with integrated magnetics," in *Proc. IEEE Appl. Power Electron. Conf. Expo.*, Anaheim, CA, USA, Feb. 2007, pp. 955–961.

[16] B. G. Kang, C. S. Park, and S. K. Chung, "Integrated transformer using magnetic sheet for LLC resonant converter," *Electron. Lett.*, vol. 50, no. 10, pp. 770–771, May 2014.

[17] M. Li, O. Ziwei, and M. A. E. Andersen, "High-frequency LLC resonant converter with magnetic shunt integrated planar transformer," *IEEE Trans. Power Electron.*, vol. 34, no. 3, pp. 2405–2415, Mar. 2019.

[18] D. C. Hamill, "Lumped equivalent circuits of magnetic components: The gyrator-capacitor approach," *IEEE Trans. Power Electron.*, vol. 8, no. 2, pp. 97–103, Apr. 1993.

[19] D. C. Hamill, "Gyrator-capacitor modeling: A better way of understanding magnetic components," in *Proc. IEEE Appl. Power Electron. Conf. Expo.*, Orlando, FL, USA, Feb. 1994, pp. 326–332.

[20] S. Yang, M. Shoyama, and S. Abe, "Design of low-profile LLC resonant converter for low transformer loss," in *Proc. IEEE Region 10 Conf. (TENCON)*, Fukuoka, Japan, Nov. 2010, pp. 1301–1306.

[21] W. G. Hurley, E. Gath, and J. G. Breslin, "Optimizing the AC resistance of multilayer transformer windings with arbitrary current waveforms," *IEEE Trans. Power Electron.*, vol. 15, no. 2, pp. 369–376, Mar. 2000.

[22] Y. Jeong, G.-W. Moon, and J.-K. Kim, "Analysis on half-bridge LLC resonant converter by using variable inductance for high efficiency and power density server power supply," in *Proc. IEEE Appl. Power Electron. Conf. Expo. (APEC)*, Mar. 2017, pp. 170–177.

[23] S. Chandrasekaran, V. Mehrotra, and H. Sun, "A new matrix integrated magnetics (MIM) structure for low voltage, high current DC-DC converters," in *Proc. IEEE 33rd Annu. IEEE Power Electron. Spec. Conf.*, Cairns, QLD, Australia, Jun. 2002, pp. 1230–1235.

[24] P. Xu, Q. Wu, P.-L. Wong, and F. C. Lee, "A novel integrated current doubler rectifier," in *Proc. 15th Annu. IEEE Appl. Power Electron. Conf. Expo.*, New Orleans, LA, USA, Feb. 2000, pp. 735–740.

[25] Y.-C. Liu, C. Chen, K.-D. Chen, Y.-L. Syu, and M.-C. Tsai, "High-frequency LLC resonant converter with GaN devices and integrated magnetics," *Energies*, vol. 12, no. 9, p. 1781, May 2019.

CHUL-WAN PARK was born in South Korea, in 1988. He received the B.S. and M.S. degrees in electrical engineering from Kookmin University, Seoul, South Korea, in 2014 and 2016, respectively, where he is currently pursuing the Ph.D. degree with the Power Electronics Systems Laboratory, College of Creative Engineering. His current research interests include high frequency and high power density dc-dc converters, integrated magnetics, and multi-level resonant converter. He is a member of the Korean Institute of Power Electronics.

SANG-KYOO HAN received the M.S. and Ph.D. degrees in electrical engineering from the Korea Advanced Institute of Science and Technology (KAIST), Daejeon, South Korea, in 2001 and 2005, respectively.

For the next six months, he was a Postdoctoral Fellow with KAIST, where he developed digital display power circuits and was involved in several research activities. Since 2005, he has been a Professor of electrical engineering with the School of Electrical Engineering, College of Creative Engineering, Kookmin University, Seoul, South Korea. His research interests include high performance and low cost PDP power systems, high efficiency LED backlight drivers, high performance photovoltaic and wind-power systems, high frequency and high power density power converters, high power converters for electric vehicles, high performance battery chargers, and high power amplifiers for broadcast sound systems.

Dr. Han is a member of the Korean Institute of Power Electronics (KIPE).